The site characterization scheme of the INGV Strong-Motion Database (ISMD): overview and site classification

Mascandola C.[(1)] *, Massa M.[(1)], Lovati S.[(1)], Augliera P.[(1)]

[(1)] Istituto Nazionale di Geofisica e Vulcanologia (INGV), Via Alfonso Corti 12, 20133, Milano, Italy

*** Corresponding author: claudia.mascandola@ingv.it**

Claudia Mascandola,
Istituto Nazionale di Geofisica e Vulcanologia
Via Alfonso Corti, 12
20133, Milano
Italy
Phone: +39 02 23699 653

Abstract

This paper describes and discusses the new site characterization scheme adopted for version 2.0 of the INGV (Italian National Institute for Geophysics and Volcanology) Strong Motion Database (ISMD), published on-line in August 2016. To date, the web portal includes more than 145,000 three-component accelerometric waveforms that have been generated by more than 1,200 Italian earthquakes with local magnitude (M_L) ≥3.0 and 213 strong-motion stations. Besides the real time distribution of accelerometric data and metadata recorded by INGV and regional partners strong motion networks, one of the main goals of ISMD is to provide a detailed characterization of recording sites from the geological, geomorphological, and geophysical points of view. ISMD allows the correct

use of these strong-motion data for a large variety of applications in engineering seismology and earthquake engineering and it allows assessing the soil and topographic categories, as indicated in the current Italian and European seismic codes.

To date ISMD represents the first repository for a homogeneous site characterization and classification for the INGV strong-motion stations, intended to be updated in relation to new available data and institutional projects.

Keywords: site characterization, site classification, strong motion data, ISMD, Italy

1. Introduction

Scientific research in the seismological and engineering fields requires strong-motion data for several purposes, such as evaluation of ground-motion models (GMPEs) and verification of shaking scenarios and probabilistic hazard maps. The correct use of accelerometric data requires detailed knowledge of instrumentation, recording sites, and seismic sources (e.g., localization, magnitude). Therefore, a web portal for strong-motion dissemination requires not only a collection of waveforms, but also the careful attribution of these metadata (Massa et al., 2014a).

In general, the behavior of the ground motion at a specific recording site depends on the source process, the propagation of the wave field in the crustal medium and the transmission of the seismic wave from the bedrock to the earth surface (i.e. free-field motion). This last contribution is known as site effect, which defines a local phenomenon that can modify the amplitude, frequency content and duration of a seismic wavefield in correspondence of particular geological or geomorphological settings. Site effects are generally considered to be the combination of the stratigraphic and topographic contributions. The former are due to the soil layers (e.g., alluvial or sedimentary cover) that overlay the bedrock and the seismic-wave amplification depends on the impedance contrast between different layers (e.g. Bard & Tucker, 1985; Bindi et al., 2009; Parolai et al., 2009; Milana et

al., 2014; Mascandola et al., 2017). These effects are often the cause of the main damages reported in several seismic crisis, where resonance effects are reported (i.e. Chávez-García and Bard 1994; Seed et al. 1991; Kawase 1996). They are usually modeled by one-dimensional (1D) wave propagation through the soil column, although when lateral heterogeneities in the elastic and/or geometrical properties are not negligible (e.g., border effects, small valleys), 2D or 3D geometries are more appropriate to describe the complexity of the ground-motion characteristics (Field, 1996; Chávez-García et al., 1999; Kawase, 1996; Bindi et al., 2009; Di Giulio et al., 2016).

The topographic effects are due to the geomorphology of the installation site, with different ground shaking depending on the ridges position and the slope extent (e.g. Griffiths & Bollinger, 1979; Géli et al., 1988; Köhler et al., 2011; Pischiutta et al., 2010; Massa et al., 2014b; Rai et al., 2016). Although there is less evidence compared to stratigraphic effects, it has been widely demonstrated that the topographic setting can produce non-negligible 2D or 3D site effects. This indicates a remarkable amplification of ground motion at the top of hills, ridges and crests, polarized along a direction perpendicular to the main axis of the topographic irregularity (Massa et al., 2014b).

In Italy, the impact of site effects on the distribution and intensity of damage has been recognized during recent important earthquakes (i.e. Accumoli, 24th August 2016, Mw 6.0; Finale Emilia, 20th May 2012, Mw 5.8; L'Aquila, 6th April 2009, Mw 6.1; http://cnt.rm.ingv.it), and in different geological and morphological contexts (Masi et al., 2016; Cultrera et al., 2016; Gallipoli et al., 2013; Ameri et al., 2009; Bordoni et al., 2012, Luzi et al., 2013).

The current Italian seismic regulations (*Nuove Norme Tecniche per le Costruzioni*; NTC, 2008) take into account the seismic site effects through the definition of soil (A, B, C, D, E, S_1,S_2) and topographic (T1, T2, T3, T4) categories, with corresponding site coefficients (S_s and S_t respectively) to evaluate the seismic actions on buildings. The soil categories are evaluated based on the mean shear-wave velocity in the uppermost 30 m (V_{S30}), or on proxies for V_{S30}, like the standard penetration test blow-count ($N_{SPT,30}$) or the undrained shear strength of the soil ($c_{u,30}$). The topographic categories are defined based on mean slope ranges, assessable in terms of 2D simple geometries, with

amplifications ascribable to slopes steeper than 15° and elevation difference (from base to top) greater than 30 m (*Nuove Norme Tecniche per le Costruzioni*; NTC, 2008).

In this paper, the site characterization scheme adopted to classify the INGV and regional partners strong-motion networks is summarized and discussed. Together with the geological, geomorphological and geophysical information, the results are now published as part of the INGV real-time Strong Motion Database (ISMD; v2.0; see *Data and Resources*).

2. Italian strong motion data sharing

In Italy, strong-motion monitoring is carried out through two national networks: the Italian National Strong-Motion Network (RAN; see *Data and Resources*), run by the Italian Department of Civil Protection and the National Seismic Network (RSN; see *Data and Resources*), run by INGV. The RAN strong-motion data for earthquakes with $M_L \geq 3.0$, recorded since 1972, are freely available from the ITalian ACcelerometric Archive (ITACA; see *Data and Resources*), while the RSN strong-motion data for earthquakes with $M_L \geq 3.0$, recorded since January, 1st, 2012, are freely available from ISMD (see *Data and Resources*). These two strong-motion databases are characterized by a different aim and philosophy. While ISMD publishes the real-time strong-motion data recorded by the permanent and temporary stations of the RSN network, ITACA provides once a year the manually post-processed data recorded by the RAN network, even if since 2014 a set of RSN stations has also been included in the database.

At the European scale, the related counterpart of ISMD is the Rapid Raw Strong-Motion (RRSM) database (see *Data and Resources*), whereas the Engineering Strong-Motion (ESM) database (see *Data and Resources*) is the related counterpart of ITACA.

3. Site characterization overview

On the ISMD web-portal, the site characterization analysis is performed for the accelerometric stations of the INGV RSN and regional partnerships (Table 1). A general overview of the stations

and the corresponding recording sites is available on the *Home-Station* page (Fig. 1a), where the site characterization sector is summarized in different thematic Tables (i.e., geology, morphology, geophysics, seismic regulations). A basic approach to site characterization is provided with geological and geomorphological maps and classifications, as well as passive geophysical analyses with single station records and microtremor arrays when available. Finally, the soil and topographic classes are assessed, as indicated in the current Italian (NTC, 2008) and European (CEN, 2003) seismic codes for buildings.

The site characterization for a specific station can be found in the corresponding *Specific-Station* page (see Fig. 1b for a sample station). It is possible to access each specific site by directly consulting the *Home-Station* page (Fig. 1a), or by queries performed through the specific *Station search* tool.

On each *Specific-Station* page, the instrumentation and the site characterization information are provided in two different tables and the waveforms recorded by that specific station from 2012 to date are downloadable in SAC-raw format only (i.e., *auto* version) for earthquakes with M_L <3.5, and both in SAC-raw format and ASCII corrected format (i.e., *revised* version) for earthquakes with local (M_L) or moment (M_w) magnitude ≥3.5 (i.e. ≥ 4.0 before 1st January 2017).

3.1. Geological characterization

For each recording site, the geological map at a 1:100,000 scale (*Società Geologica Italiana*; SGI, see *Data and Resources*) is provided, with topographic base at 1:25,000 scale (Istituto Geografico Militare; IGM, see *Data and Resources*). The geological maps at a 1:50,000 scale (CARG project; see *Data and Resources*) are also provided for a few sites and they will be implemented when available.

To facilitate queries on ISMD, different geological classes, as illustrated in Figure 2a, are formulated. The different lithologies are grouped into three main classes of rocks: sedimentary, metamorphic and igneous; whereas deposits (i.e. unconsolidated quaternary sediments) are grouped

into sedimentary, volcanic, morainic and debris-slope (Fig. 2a). The different classes of rocks and deposits imply different geological processes. In particular, the *Sedimentary-cover* implies fluvial deposition, including all of the alluvial, fluvio-glacial, and lacustrine deposits, whereas the *Volcanic-*, *Morainic-* and *Debris-slope* deposits imply volcanic, glacial and slope erosion processes, respectively. The subdivision into geological classes is meant to be functional for the expected different seismic responses.

The INGV strong-motion stations are mostly installed on sedimentary rock or sedimentary cover, as shown in Figure 2a for 86% of the stations. The sites classified in *Sedimentary-cover* are mainly on the Po Plain, whereas those in *Sedimentary-rock* are mainly along the Apennines, with a few in the Central and Eastern Alps (Fig. 2b). The remaining few stations are distributed in the other geological classes (Fig. 2a). The sites classified into *Volcanic-deposits* are in Sicily or central Italy, those into *Morainic-deposits* are sited along the Alps, whereas those classified into *Debris-slope* are along the Alps and central Apennines. Sites classified in *Metamorphic-* and *Igneous-rock* can be found along the Alps, but also along both the northern and southern Apennines (Fig. 2b).

3.2. Geomorphological characterization

For each recording site, three different maps are proposed to characterize the geomorphological setting: the digital elevation model (DEM) map, the topographic map (i.e., *Slope*, *Ridge*) and the 3D Google Earth (see *Data and Resources*) map.

The geomorphological analysis was performed following Pessina and Fiorini (2014). In that paper, the authors propose a GIS procedure for fast topographic characterization of seismic recording stations, using a 1″ resolution ASTER Global DEM V2 (see *Data and Resources*) and elaborating critical slope and ridge detection maps from the DEM. Moreover, they performed a test on different raster resolutions, concluding that, as a general rule, the 20 m resolution seems to be a good compromise between detail of the map produced and computational time. The authors state that the

20 m resolution of the DEM is comparable to the smaller feature width required by the Italian building code (NTC, 2008) and that no important ridges should be overlooked (Pessina and Fiorini, 2014). Therefore, the geomorphological analysis for ISMD was carried out in ArcGIS[1], projecting[2] the ASTER GDEM with a cell size of 20 m (in Italy, an arc-second of longitude varies between 21 m to 24 m). Afterwards the DEM was corrected to remove unnatural sinks[3] in order to be hydrologically correct. In general, natural sinks are local minimums where the flow concentrates, but they are rare in natural environments and they are often due to errors in the DEM generation process (Pessina and Fiorini, 2014). Subsequently, a smoothing was performed by applying a mean algorithm with a 3 × 3 moving window, to remove small irregularities[4].

Starting from the processed DEM, the slope map was constructed[5] with three classes (0-15°; 15-30°; >30°), considering the break values defined in the current Italian seismic code (NTC, 2008). The ridgelines were extracted using the Topographic Position Index (TPI) algorithm (Jeff Jenness: online TPI documentation, see *Data and Resources*; Weiss, 2001). With respect to Pessina and Fiorini (2014), we used the TPI algorithm because less influenced by the DEM quality and artefacts. The TPIs reflect the differences between the elevation in a particular cell and the mean elevations of the cells around that cell. This kind of analysis is naturally very scale dependent. The scale is determined by the neighborhood used in the analysis, which defines what cells are considered to be "around" that cell. To set the neighborhood interval for the TPI analysis, different tests were carried out considering different radii (i.e. 300 m, 500 m and 800 m). In our case, a neighborhood circle with a radius of 500 m was adopted, as allowed to better discriminate the crests of the main ridges, while ignoring the minor deflections. The TPIs are then subdivided into three classes with the *Natural Breaks* method in ArcGIS. The class with the higher values corresponds to the ridge zones that are extractable from

[1] ESRI 2011. ArcGIS Desktop: Release 10. Redlands, CA: Environmental Systems Research Institute.
[2] tool: *Project Raster* in *Data Management/Projections and Transformations/Raster*
[3] tool: *Fill* in *Spatial Analyst Tools/Hydrogeology*
[4] tool: *Focal Statistics* in *Spatial Analyst Tools/Neighborhood*
[5] tool: *Slope* in *Spatial Analyst Tools/Surface*

177 the TPI map with a simple query[6]. Applying a thinning function[7] (thins rasterized linear features by
178 reducing the number of cells representing the width of the features; Zhan C., 1993) to the ridge zones,
179 the ridgelines can be obtained and then plotted on the slope map, composing the topographic maps
180 now available on the ISMD web portal.

181 In addition to the graphical output, to facilitate queries on ISMD, a morphological
182 classification was formulated and each station classified based on the morphology classes illustrated
183 in figure 2c. The formulated classes were: *Plain*, *Valley* and *Plateau*, to discriminate between
184 different flat morphologies; *Ridge*, *Relief* and *Gentle-slope*, to discriminate between different slopes.
185 This distinction is made to be functional to different expected seismic response. In particular, the flat
186 morphologies do not present a topographic amplification, but can be interested by a significant soil
187 amplification that can vary according to different geological setting. Therefore, the term *Plain*
188 includes all of the stations installed in the Northern Italy Plains, as well as those along the Adriatic
189 coast, where the geological model is approximately 1D (e.g. Mascandola et al., 2017; Milana et al.,
190 2014). *Valley* includes stations installed in correspondence with both Alps and Apennine
191 intermountain valleys or small basins, generally modeled with 2D or 3D geometries (e.g. Bindi et al.,
192 2009). The term *Plateau* includes instead a restricted set of morphological settings, such as that
193 located in the Puglia region (Southern Italy), where extended flat morphologies are formed by
194 outcropping rocks. The not flat morphologies can instead be interested by a topographic amplification
195 that can vary according to the different geomorphology of the site. Therefore, the term *Ridge* indicates
196 those morphologies with a crest much narrower than the base, exactly as the current Italian seismic
197 code (NTC, 2008) describes the T3 and T4 topographic classes. For these cases, the expected
198 topographic amplification is higher than the other morphologies with extended top, indicated with
199 *Relief* in the ISMD morphology classification and corresponding to the T2 topographic class,

[6] tool: *Raster Calculator* in *Spatial Analyst Tools/Map Algebra*
[7] tool: *Thin* in *Spatial Analyst Tools/Generalization*

200 described in the current Italian seismic code (NTC, 2008). The term *Gentle-slope* is instead defined
201 for those sites in T1 class with hillslopes <15° and therefore no topographic amplification expected.
202 Subsequently, a *position* field is required for those morphology classes that can present a different
203 seismic response depending on position. In case of topographic influence, slope and crest generally
204 present different amplifications (e.g. Griffiths & Bollinger, 1979; Géli et al., 1988; Köhler et al.,
205 2011; Pischiutta et al., 2010; Massa et al., 2014b), whereas in case of plains or small basins, different
206 amplifications are expected at the edge, for the contribution of basin-edge-induced waves,
207 horizontally propagating within the basin (Field, 1996; Kawase, 1996; Di Giulio et al., 2003; Di
208 Giulio et al., 2016; Bindi et al., 2009). Therefore, stations in *Plain* and *Valley* are discriminated
209 between *edge* and *center*, with the addition of *coast* for *Plain*. Stations for *Ridge* are instead
210 subdivided into *slope* and *crest* positions, as well as those for *Relief*, where the term *crest* is replaced
211 with *top* to distinguish between the *Ridge* narrow crest and the flat extended top of the *Relief*. The
212 *Gentle-slope* class does not have a position subdivision because of the much-smoothed morphology.
213 The position class is defined based on a visual inspection of the slope and ridge map, besides the
214 Google Earth view and the available photographic documentations. According to this classification,
215 most of the recording sites (77%) are *Ridge*, *Relief*, *or Gentle-slope*, with prevalence of *Relief* (35%)
216 (Fig. 2c). The stations in *Relief* are equally distributed between *top* and *slope*, whereas the stations in
217 *Ridge* are mainly *crest* (Fig. 2c). Stations in *Valley* are equally distributed between *edge* and *center*,
218 whereas those in *Plain* are mainly *center*, with just a few along the Adriatic coast (i.e., MESG, SENI,
219 VENL). Geographically, these morphology classes are distributed along both the Alps and the
220 Apennines, except for the *Gentle-slope* class, which is concentrated along the Apennines, and the
221 *Plain* class, which is concentrated in the Po Plain area (Fig. 2d).
222 The association between the topographic classes of the European and National seismic codes with the
223 morphological classes defined for ISMD is shown in figure 3. In particular, the flat morphologies
224 with no amplification expected (topographic site coefficient (S_t) = 1.0; NTC 2008) are always
225 included in T1 class. In this case, the position defined for *Plain* and *Valley* can be indicative of

different stratigraphic and basin effects (i.e. of basin-edge-induced waves). On the other hand, the different slopes are subdivided based on different slope classes and simple morphologies illustrated in the seismic codes (NTC 2008; CEN 2003), as shown in figure 3. Therefore, all stations classified in *Relief* are included in T2 class, whereas all stations classified in *Ridge* are included in T3 or T4 classes. In these cases, the position is indicative of different topographic site coefficients (S_t), ranging from 1.0 at the foot, to 1.1 or 1.2 along the hillside and 1.2 or 1.4 at the crest/top of the slope (Fig. 3).

3.3. Geophysical characterization

The results of the geophysical analyses are based either on microtremor data recorded by enlarged-band (Lennartz 5s, see *Data and Resources*) or broad-band (Trillium 40s, see *Data and Resources*) velocimeters installed in correspondence with six-channel RSN seismic stations, or on ambient noise temporary measurements performed in correspondence with three-channel accelerometric stations. For the recording sites where velocimetric measurements are not available (17%), the geophysical analysis was not performed because accelerometers cannot define the noise frequency content well, especially at low frequencies (i.e., Mucciarelli, 1998; SESAME Guidelines, see *Data and Resources*).

In general, for each ISMD strong-motion station, the HVSRs (Nakamura, 1989) are presented in the form of standard curves (squared average of the horizontal components over the vertical) and rotated HVSRs, computed from the horizontal component rotation, to define potential site polarizations in site amplification effects. The analyses are performed considering signals at least 24 h long, with sub-windows of 60 s or 120 s. In particular, 120 s are preferred in case of low frequency peaks (i.e., <1.0 Hz), which are mainly seen in correspondence with deep alluvial basins (i.e., the Po Plain). Moreover, a 5% tapering was applied together with a Konno & Omachi (1998) smoothing with b=20. To appreciate the H/V sensitivity to different smoothing levels (i.e., b = 20, 40) and window lengths (i.e., 60, 120 s), an example is shown in Figure 4. In general, while the influence of smoothing is more appreciable for high frequency peaks (Fig. 4*a*, *b*), the window length has more

influence on amplification at frequencies <1 Hz, where the use of 120 s allows us to reduce the variability of the results (Fig 4*c*, *d*).

The f_0 published on ISMD always correspond to the lowest frequency peak, characterized by amplitude (A) ≥2, as indicated in the SESAME guidelines (see *Data and Resources*). The attribute *none* indicates a flat (A ≤2) HVSR response in the frequency range of 0.1-15 Hz. Together with the f_0, a field of *Notes* is provided for comments on the geophysical analysis presented. Every ambient noise HVSR on ISMD meets the requirements of the first class of SESAME criteria (see *Data and Resources*), relating to the *reliability of the H/V curve*. On the other hand, the second class of SESAME criteria (see *Data and Resources*), relating to the *clear H/V peak*, is not always verified, in particular in the presence of peaks with low amplitude value or in case of broad range of amplified frequencies (i.e. large H/V peaks). Figure 5 shows an example of a clear H/V peak Vs a non-clear H/V peak. Figure 5a presents a clear H/V peak at 0.25 Hz for station OPPE (Oppeano), which was installed on a flat topography (Po Plain), whereas figure 5b presents an example of a non-clear H/V peak at 3.2 Hz for station BULG (Bulgheria Camerota), which was installed on a *Ridge* (southern Apennines). In this case, the large H/V peak can be due to the irregularities in the geomorphology, which can slightly amplify a large range of frequencies, to result in no clear H/V peaks. This effect was indeed observed for several stations on slope, currently on ISMD, but also other influences might combine with the topographic effect (e.g., the presence of colluvial layers or structural anisotropies, Marzorati et al., 2011). However, it is well known that the topographic amplifications are usually polarized in the direction perpendicular to the ridge elongation (Massa et al., 2014b; Lovati et al., 2011; Buech et al., 2010; Burjanek et al., 2010; Pischiutta et al., 2010). This characteristic can be seen in figure 5d, where the amplification in correspondence with station BULG is mainly oriented in N-S direction and involves a broad frequency range (1-10 Hz) that is characterized by variable amplitude. On ISMD, the non-clear peaks are also indicated as f_0, as soon as they reach amplitudes (A) of 2.

In addition to the HVSRs from single-station measures, the shear wave (V_S) velocity profiles, together with the V_{S30} values, are now available for stations CDCA, CMPO, CTL8, FERS, FIVI, LAV9, MILN, NDIM, ROM9, SANR. The results were obtained from active- or passive-source surface wave methods performed over the last years, thanks to several agreements between INGV and Italian Civil Protection (DPC). This additional information is meant to be updated and implemented in the near future.

3.4. Site classification assessment

As now indicated by the Italian seismic code for building (NTC, 2008) and the Eurocode8 (CEN, 2003), both soil and topographic categories are provided for each recording site, based on previous analyses.

The soil category (Table 2) can be assigned considering the lithology and the mean V_{S30} or its proxies, such as the standard penetration test blow-count ($N_{SPT,30}$) and the undrained shear strength of the soil ($c_{u,30}$). Due to the general lack of measured V_{S30} values for the target sites, the soil categories were assigned from the surface geology information, considering the classification proposed by Di Capua et al. (2011a,b), marked with the symbol ***** (asterisk) on the ISMD website. As also indicated by Felicetta et al. (2016) for the ITACA database, the near-surface geology can be a non-optimal proxy for the geophysical properties of a site. In particular, taking advantage of the comparison with V_{S30} measures, they showed that soil class B includes the largest error (approximately 60%). Therefore, the soil classes estimated with reference to Di Capua et al. (2011a,b) do not provide accurate data, but certainly provide a first level of knowledge. In this sense, when detailed studies (e.g., active or passive geophysical prospections) are available in the surroundings of the station installation site, they are taken into account for modification of the reference classification. Based on an expert judgment, these cases are indicated with the symbol ****** (double asterisks) on the ISMD website.

Figure 6a shows that the majority of the ISMD seismic stations were installed on sites in class A (69 on rock and 4 on morainic deposits) or on sites in class B (83 on rock and 23 on sedimentary, volcanic and slope deposits). Of the sites in class C and D, all are *Sedimentary-cover,* except for 2 in class C, which are *Debris-slope.*

The topographic categories can be assigned considering the heights and slopes of simple 2D relief configurations and four classes of topographic amplification are explicitly defined, as listed in Table 3. The topographic categories (Table 3) are initially assigned considering the semi-automatic method proposed in Pessina and Fiorini (2014). It is worth noting that ASTER DEM standard data products have Z accuracies generally between 10 m and 25 m root mean square error (ASTER Global DEM Validation, Summary Report; see *Data and Resources*), that may influence the semi-automatic classification, especially for those geometries that are nearly 30 m high. Moreover, the semi-automatic method is not always able to directly classify a site. In that cases the output is *NC* (i.e., not classified) and a manual revision is necessary to assign a topographic category. However, a review of the semi-automatic classification was performed for each station, in order to verify the classification and overcome the uncertainties related to the semi-automatic procedure and to the DEM vertical error. The manual revision was performed measuring the mean slope angle on Google Earth (see *Data and Resources*) and looking at the general morphology of the installation site. In case of slopes with different gradients, the higher slope angle was considered since it is more conservative for the site-effects evaluation. To identify the variations with respect to the output of the semi-automatic method, the symbol ***** (asterisk) and the symbol ****** (double asterisks) were introduced on the ISMD website to indicate the sites that were not directly classified (i.e. *NC* output) and the changes with respect to the semi-automatic output, respectively. The statistics in Figure 6b illustrate that the majority of the ISMD stations were installed in sites classified in T1 or T2; highlighting that the semi-automatic procedure of Pessina and Fiorini (2014) can better classify sites in T1, whereas it has difficulties in particular with sites in T2, where there are more *NC* outputs (*) and modified outputs

(**). However, it is worth noting that the topographic class is not always easy to assign following the indications in the current seismic code, especially in those cases were the topography is complex and not well defined in simple 2D relief configurations.

Figure 6c, d shows the station distribution with the relative topographic and soil classes. A striking observation is that T1 and T2 classes characterize most of the stations in the Apennine range, although looking at the soil classes, the same stations are mainly classified in B or A. This is probably due to the smoothed topography that characterizes the Apennine range, with respect to the Alps, where the correspondence between topographic and soil classes is more consistent (sites in A or B are also classified as T2, T3, or T4). The stations in the Po Plain are instead classified equally in C and T1, except for two stations located near the Adriatic coast, which are classified in D.

4. Discussion and conclusions

The correct evaluation of seismic-site response is fundamental to the correct interpretation of accelerometric waveforms. For this reason, the characterization of the recording sites is a key issue when compiling strong-motion databases. In this paper, the site characterization scheme developed over the last years and now adopted to classify the recording sites for the ISMD real time database (see *Data and Resources*) is summarized and discussed.

Correlating the observations of the above paragraphs, some general considerations can be formulated. As shown in Figure 7a, about 70% of the stations were installed on rocky sites, while the remaining falls on deposits. In particular, the majority of the stations were installed on *Sedimentary-rock*, in classes A or B, and on *Sedimentary-cover* in classes B, C, or D. Concerning the geomorphological classification (Fig. 7b), about 75% of the stations were installed on *Gentle-slope* (class T1), *Ridge* (classes T3 and T4) or *Relief* (class T2), while just the 25% of the stations were installed on *Plain, Valley* or *Plateau,* in T1 class. In Figure 7c, the NTC (2008) topographic and stratigraphic classes are combined to emphasize the distribution and correlation between the different classes. The sites in class T1 are distributed in all of the soil categories: 15% in class A, 52% in class

B, 31% in class C, and 2% in class D. In detail, sites in T1 and A or B soil classes are in *Valley* (in the *edge* position*)* or *Gentle-slope* morphology classes, with just a few stations in *Plain* and *Plateau*. On the other hand, sites in T1 and C or D soil classes are mainly in *Plain* or *Valley,* as expected. Sites in T2, T3 and T4 classes are nearly equally distributed in A and B soil classes. The combination of so many A and B in T1 (about 30%) might be indicative of possible uncertainties both in topographic and soil categories. The former may be due to difficulties in matching simple 2D relief configurations with the natural complex geomorphologies; the latter may be due to the scarce availability of quantitative V_{S30} measurements, besides the lack of detailed geological information.

In Figure 8, the f_0 values are correlated to the geological (Fig. 8a) and geomorphological (Fig. 8b) characterization. Figure 8a shows that rocky sites generally present a flat H/V response (or $f > 10$ Hz), except for the frequency range 1-5 Hz, where the amplifications are often associable to the topographic contribution or to the presence of thin sedimentary covers. Instead, about 50% of the deposits shows amplifications at frequencies $f < 1$ Hz, denoting the behavior of the recording sites in the Po Plain (e.g., Mascandola et al., 2017; Massa et al., 2016; Milana et al., 2014; Massa and Augliera, 2013; Luzi et al., 2013; Marzorati and Bindi, 2006), mainly classified in C or D classes. The f_0 values on deposits, in the range 1-10 Hz (29%), reflect in general the sites at the edge of plains or in small inter-mountain valleys, which are often classified in B and C soil classes. The stations in class A with a flat H/V response (about 60%) are those on *Morainic-deposits* or *Sedimentary-*, *Metamorphic-* and *Igneous-rock,* whereas those with H/V peaks are only on *Sedimentary-rock.* Sites in class B with flat H/V response include *Volcanic-deposits,* and *Sedimentary-*, *Metamorphic-* and *Igneous-rock*, even if the *Sedimentary-rock* (i.e. mainly marls and limestone) prevails over the others. Sites in class B with H/V peaks are instead those on *Sedimentary-cover* and *Volcanic-deposits,* with few cases on *Sedimentary-rock* (i.e. mainly conglomerate and sandstone).

The statistics for the geomorphological characterization are presented in Figure 8b, where the similarity with the geological characterization (Fig. 8a) is not surprising, as in general flat morphologies correspond to sedimentary basins and slope morphologies are characterized by

outcropping rocks or thin sedimentary layers. In this case, while flat morphologies in T1 class show amplifications in a wide frequency range (0.1-10 Hz), sites in T2, T3 and T4 are mainly distributed in a narrow range (1-5 Hz) or do not show any amplification at all. In particular, as shown in Figure 8a for rock, many sites on slopes show H/V peaks in the range of 1-5 Hz, highlighting how, particularly for this range of frequency, sites can be affected by amplifications that need to be considered in the reference rock-site identification. In agreement with the recent literature (Massa et al., 2014b; Lovati et al., 2011; Buech et al., 2010; Burjanek et al., 2010; Pischiutta et al., 2010), stations classified in T3 or T4 show H/V peaks often polarized in the directions perpendicular to the main elongation of the ridge.

The large variability observable from the H/V data, at stations classified in the same soil (in particular A and B classes) or topographic class (NTC, 2008; CEN 2003) might be a warning of possible uncertainties in the final class association. However, the site characterization for the INGV strong motion stations is continually in progress, in relation to new available data or institutional projects (e.g. CRISP, Cultrera et al., 2017). At present, while the geophysical characterization is constantly updated as soon as better quality measures are available, the geological section will be implemented with more geological maps at 1:50,000 scale, provided by the CARG project (see *Data and Resources*) and the geomorphological section will be updated with the TinItaly DEM (Tarquini et al., 2007, 2012), with a 10-m cell size that allows a better resolution in the Italian territory. In light of these new upgrades, the topographic and soil categories (NTC, 2008; CEN 2003) will also be reviewed and updated. The current site classification is available on the ISMD web site (see *Data and Resources*), in addition to the electronic supplement (Table S1), where the current soil and topographic categories are listed for the 213 strong-motion stations now published on ISMD.

Data and Resources

The web portal described in this work is published at http://ismd.mi.ingv.it/

The others web sites cited in the paper are:

ftp://ftp.geo.uib.no/pub/seismo/SOFTWARE/SESAME/USER-GUIDELINES/SESAME-HV-User-Guidelines.pdf (SESAME Guidelines, European research project WP12 – Deliverable D23.12 (2004)),

http://cnt.rm.ingv.it/en/instruments/network/IV (RSN; National Seismic Network),

http://esm.mi.ingv.it/ (ESM; Engineering Strong Motion database),

http://gdex.cr.usgs.gov/gdex/ (ASTER Global DEM V2),

http://itaca.mi.ingv.it/ (ITACA; DPC ITalian ACcelerometric Archive),

https://lpdaac.usgs.gov/sites/default/files/public/aster/docs/ASTER_GDEM_Validation_Summary_Report.pdf (ASTER Global DEM Validation, Summary Report),

http://www.igmi.org/prodotti/cartografia/carte_topografiche/ (IGM; Istituto Geografico Militare),

http://www.isprambiente.gov.it/it/cartografia/ (SGI, Società Geologica Italiana, Carta geologica d'Italia 1:100000),

http://www.isprambiente.gov.it/it/progetti/suolo-e-territorio-1/progetto-carg-cartografia-geologica-e-geotematica (CARG project; Geological CARtography, *CARtografia Geologica*),

http://www.jennessent.com/arcview/tpi.htm (Jeff Jenness TPI documentation),

http://www.lennartz-electronic.de/ (Lennartz 5s, Lennartz instruments),

http://www.nanometrics.ca/ (Trillium 40s, Nanometrics instruments),

http://www.protezionecivile.gov.it/jcms/it/ran.wp (RAN web site),

https://www.google.com/earth (Google Earth),

www.orfeus-eu.org/rrsm/ (RRSM; Rapid Raw Strong Motion database).

Last accessed for all web sites: 31st May 2017.

Acknowledgments

We are grateful to the Editor In Chief Zhigang Peng, the Associate Editor and the anonymous reviewers for their thorough review and precious suggestions, which brought a significant improvement to the work.

References

Ameri G., Massa M., Bindi D., D'Alema E., Gorini A., Luzi L., Marzorati M., Pacor F., Paolucci R., Puglia R., Smerzini C. (2009). The 6 April 2009, M_w 6.3, L'Aquila (Central Italy) earthquake: strong-motion observations. Seism. Res. Lett., 80, 6, 951-966.

Bard P. Y. and Tucker B. E. (1985). Underground and ridge site effects: a comparison of observation and theory. Bull. Seism. Soc. Am., 75, 905-922.

449 Bindi D., Parolai S., Cara F., Di Giulio G., Ferretti G., Luzi L., Monachesi G., Pacor F., Rovelli A.
450 (2009). Site amplifications observed in the Gubbio basin (Central Italy): hints for lateral propagation
451 effects. Bull. Seism. Soc. Am., 99, 2A, 741–760.
452
453 Bordoni P., Azzara R., Cara F., Cogliano R., Cultrera G., Di Giulio G., Fodarella A., Milana G.,
454 Pucillo S., Riccio G., Rovelli A., Augliera P., Luzi L., Lovati S., Massa M., Pacor F., Puglia R., Ameri
455 G. (2012). Preliminary result from EMERSITO, the rapid response network for site effect studies.
456 Ann. Geophys., 55, 4, 829-835.
457
458 Buech F., Davies T. R., Pettina J. R. (2010). The little red hill seismic experimental study: topographic
459 effects on ground motion at a bedrock-dominated mountain edifice. Bull. Seism. Soc. Am., 100, 5,
460 2219-2229.
461
462 Burjanek J., Gassner-Stamm G., Poggi V., Moore J. R., Fah D. (2010). Ambient vibration analysis of
463 an unstable mountain slope. Geophys. J. Int., 80, 820-828.
464
465 CEN (2003), prEN 1998-1- Eurocode 8: design of structures for earthquake resistance. P1: General
466 rules, seismic actions and rules for buildings. Draft 6, Doc CEN/TC250/SC8/N335.
467
468 Chávez-García F.J. and Bard P.Y. (1994). Site effects in Mexico city eight years after the September
469 1985 Michoacan earthquakes. Soil Dyn. Earth. Eng., 13, 229-247.
470
471 Chávez-García F.J., Stephenson W.R., Rodriguez M. (1999). Lateral propagation effects observed at
472 Parkway, New Zeland. A case history to compare 1D to 2D site effects. Bull. Seismol. Soc. Am., 89,
473 718- 732.

Cultrera G., D'Alema E., Amoroso S., Angioni B., Bordoni P., Cantore L., Cara F., Caserta A., Cogliano R., D'Amico M., Di Giulio G., Di Naccio D., Famiani D., Felicetta C., Fodarella A., Lovati S., Luzi L., Mascandola C., Massa M., Mercuri A., Milana G., Pacor F., Pischiutta M., Pucillo S., Puglia R., Riccio G., Tarabusi G., Vassallo M. (2016). Site effect studies following the 2016 Mw 6.0 Amatrice earthquake (Italy): the Emersito Task Force activities. Ann. Geophys., 59, fast truck 5, doi: 10.4401/ag-7189.

Cultrera G., Cardinali M., De Franco R., Gallipoli M.R., Pacor F., Pergalani F., Milana G., Moscatelli M. & Amatrice working group (2017). Site effects in the Amatrice municipality through dense seismic network and detailed geological-geophysical survey, EGU, 23–28 April 2017, Wien, Austria.

Di Capua G., Lanzo G., Pessina V., Peppoloni S., Scassera G. (2011a). The recording stations of the Italian strong motion network: geological information and site classification. Bull. Earthq. Eng., 9, 1779-1796.

Di Capua G., Peppoloni S., Amanti M., Cipolloni C., Conte G., Avola D., Del Buono A., Borgomeo E., Negri Arnoldi C., Scrivieri. S (2011b). Il progetto SEE-GeoForm: uno strumento per la consultazione di dati geologici e di pericolosita` sismica riferiti all'intero territorio nazionale. In: Proceedings of the XIV conference ANIDIS, Bari 18-22 September 2011.

Di Giulio G., Rovelli A., Cara F., Azzara R. M., Marra F., Basili R., Caserta A. (2003). Long-duration asynchronous ground motions in the Colfiorito plain, central Italy, observed on a two-dimensional dense array. J. Geophys. Res. 108, no. B10, 2486, doi 10.1029/2002JB002367.

Di Giulio G., De Nardis R., Boncio P., Milana G., Rosatelli G., Stoppa F., Lavecchia G. (2016). Seismic response of a deep continental basin including velocity inversion: the Sulmona intramontane basin (Central Apennines, Italy). Geophys. J. Int., 204, 1, 418-439.

Felicetta C., D'Amico M., Lanzano G., Puglia R., Russo E., Luzi L. (2016). Site characterization of Italian accelerometric stations. Bull. Earthq. Eng., DOI 10.1007/s10518-016-9942-3.

Field E.H. (1996). Spectral amplification in a sediment-filled valley exhibiting clear basin-edge-induced waves. Bull. Sesimol. Soc. Am., 86, 991-1005.

Gallipoli M. R., Bianca M., Mucciarelli M., Parolai S., Picozzi M. (2013). Topographic versus stratigraphic amplification: mismatch between code provisions and observations during the L'Aquila (Italy, 2009) sequence. Bull. Earthq. Eng., 11, 5, 1325-1336.

Géli L., Bard P.Y., Jullien B. (1988). The effect of topography on earthquake ground motion: a review and new results. Bull. Seism. Soc. Am., 78, 42-63.

Griffiths D. W. and Bollinger G. A. (1979). The effect of Appalachian Mountain topography on seismic waves. Bull. Seism. Soc. Am., 69, 1081-1105.

Kawase H. (1996). The cause of the damage belt in Kobe: the basin-edge effects, constructive interference of the direct S-wave with the basin-induced diffracted/Rayleigh waves. Seismol. Res. Lett. 67: 25-34.

Köhler A., Weidle C., Maupin V. (2011). On the effect of topography on surface wave propagation in the ambient noise frequency range. Journ. Seism., doi:10.1007/s10950-011-9264-5.

525

526 Konno K., Ohmachi T. (1998). Ground-motion characteristics estimated from spectral ratio between
527 horizontal and vertical components of microtremors. Bull. Seism. Soc. Am., 88, 228-241.

528

529 Lovati S., Bakavoli M. K. H., Massa M., Ferretti G., Pacor F., Paolucci R., Haghshenas E., Kamalian
530 M., (2011). Estimation of topographical effects at Narni ridge (Central Italy): comparisons between
531 experimental results and numerical modelling. Bull. Earth. Eng., 9, 6, 1987-2005.

532

533 Luzi L., Pacor F., Ameri G., Puglia R., Burrato P., Massa M., Augliera P., Castro R., Franceschina
534 G., Lovati S. (2013). Overview on the strong motion data recorded during the May-June 2012 Emilia
535 seismic sequence. Seism. Res. Lett., 84, 4, 629-644.

536

537 Marzorati S., Bindi D. (2006). Ambient noise levels in north central Italy, G-Cube, 7, 9, 1-14.

538

539 Marzorati S., Ladina C., Falcucci E., Gori S., Ameri G., Galadini F. (2011). Site effects "on the rock":
540 the case of Castelvecchio Subequo (L'Aquila, Cnntral Italy). Bull. Earth. Eng., 9, 3, 841-868.

541

542 Mascandola C., Massa M., Barani S., Lovati S., Santulin M. (2017). Long-period amplification in
543 deep alluvial basins and consequences for site-specific probabilistic seismic hazard analysis: an
544 example from the Po Plain (northern Italy). Bull. Seism. Soc. Am., doi: 10.1785/0120160166.

545

546 Masi A., Santarsiero G., Chiauzzi L., Gallipoli M. R., Piscitelli S., Vignola L., Bellanova J., Calamita
547 G., Perrone A., Lizza C., Grimaz S. (2016). Different damage observed in the villages of Pescara del
548 Tronto and Vezzano after the M6.0 August 24, 2016 central Italy earthquake and site effects analysis.
549 Ann. Geophys., 59, fast truck 5, doi: http://dx.doi.org/10.4401/ag-7271.

550

551 Massa M. and Augliera P. (2013). Teleseisms as estimator of experimental long period site
552 amplifications: example in the Po Plain (Italy) from the 2011, Mw 9.0, Tohoku-Oki (Japan)
553 earthquake. Bull. Seism. Soc. Am., 103, 5, 2541-2556.
554
555 Massa M., Lovati S., Franceschina G., D'Alema E., Marzorati S., Mazza S., Cattaneo M., Selvaggi
556 G., Amato A., Michelini A., Augliera P. (2014a). ISMD, a web portal for the real time processing
557 and dissemination of INGV strong-motion data. Seism. Res. Lett., 85, 4, 727-734.
558
559 Massa M., Barani S., Lovati S. (2014b). Overview of topographic effects based on experimental
560 observations: meaning, causes and possible interpretations. Geophys. J. Int., doi: 10.1093/gji/ggt341.
561
562 Massa M., D'Alema E., Mascandola C., Lovati S., Scafidi D., Franceschina G., Gomez A.,
563 Carannante S., Piccarreda D., Mirenna S., Augliera P. (2016). The INGV real time strong motion data
564 sharing in the 2016 Amatrice (central Italy) seismic sequence. Ann. Geophys., 59, fast truck 5, doi:
565 10.4401/AG-7193.
566
567 Milana G., Bordoni P., Cara F., Di Giulio G., Hailemikael S., Rovelli A. (2014). One-dimensional
568 velocity structure of the Po River plain (northern Italy) assessed by combining strong motion and
569 ambient noise data. Bull. Earth. Eng., 12, 2195-2209.
570
571 Mucciarelli M. (1998). Reliability and applicability of Nakamura's technique using microtremors: an
572 experimental approach. Journ. Earthq. Eng., 2, 4, 625-638.
573
574 Nakamura Y. (1989). A method for dynamic characteristics estimation of subsurface using
575 microtremor or the ground surface. Quart. Rep. Rail. Tech. Res. Inst. (RTRI), 30, 1.
576

577 NTC (2008) Ministero delle Infrastrutture e dei Trasporti. Nuove Norme Tecniche per le Costruzioni.
578 Part 3: Categorie di sottosuolo e condizioni topografiche, Gazzetta Ufficiale n. 29 del 4 febbraio 2008
579 (in Italian).
580
581 Parolai S., Cara F., Bindi D. Pacor F. (2009). Empirical site-specific response-spectra correction
582 factors for the Gubbio basin (central Italy). Soil Dynam. Earthq. Eng., 29, 546-552.
583
584 Pessina V. and Fiorini E. (2014). A GIS procedure for fast topographic characterization of seismic
585 recording stations. Soil Dynam. Earthq. Eng., 63, 248-258.
586
587 Pischiutta M., Cultrera G., Caserta A., Luzi L. Rovelli A. (2010). Topographic effects on the hill of
588 Nocera Umbra, central Italy. Geophys. J. Int., 182, 2, 977–987.
589
590 Rai M., Rodriguez-Marek A., Yong A. (2016). An Empirical Model to Predict Topographic Effects
591 in Strong Ground Motion Using California Small- to Medium-Magnitude Earthquake Database.
592 Earthquake Spectra, 32, 2, 1033-1054.
593
594 Seed R.B., Dickenson S.E., Idriss I.M. (1991). Principal geothecnical aspects of the 1989 Loma
595 Prieta earthquake. Soil Found, 31, 1-26.
596
597 Tarquini S., Isola I., Favalli M., Mazzarini F., Bisson M., Pareschi M. T., Boschi E. (2007).
598 TINITALY/01: a new Triangular Irregular Network of Italy. Ann. Geophys., 50, 3,
599 http://dx.doi.org/10.4401/ag-4424.
600

601 Tarquini S., Vinci S., Favalli M., Doumaz F., Fornaciai A., Nannipieri L. (2012). Release of a 10-m-
602 resolution DEM for the Italian territory: Comparison with global-coverage DEMs and anaglyph-
603 mode exploration via the web. Computers & geosciences, 38, 1, 168-170.
604
605 Weiss A. (2001). Topographic position and landform analysis. Poster presentation, ESRI Users
606 Conference, San Diego, CA.
607
608 Zhan C. (1993). A Hybrid Line Thinning Approach. Proceedings Auto-Carto 11, Minneapolis, pp.
609 396-405.
610
611
612
613
614
615
616 **Captions**
617
618 **Figure 1 -** (a) *Home-Station* page on the ISMD web-portal (see *Data and Resources*). (b) Example
619 of *Specific-Station Page* for the CTL8 seismic station.
620
621 **Figure 2 –** Histogram of the geology classes currently on ISMD (a) and geographic distribution (b),
622 shearing the same legend of panel (a). Histogram of the morphology classes currently on ISMD (c),
623 with subsequent subdivision in position. E: edge; CE: center; C: coast; T: top; S: slope; CR: crest.
624 The geographic distribution of the morphology classes is represented in panel (d), with the same
625 legend of panel (c).
626

Figure 3 - Diagram of the morphology classification currently adopted for ISMD and association with the topographic categories of the current Italian (NTC, 2008) and European (CEN, 2003) seismic codes.

Figure 4 - Comparison between the horizontal to vertical Fourier spectral ratio curves obtained considering different smoothing (*a*, *c*: b = 20; *b*, *d*: b = 40) and window lengths, superimposed with different legend, at two sites corresponding to stations MERA (a, b) and OPPE (c, d).

Figure 5 - Examples of clear H/V peak (for station OPPE; a, c) and non-clear H/V peak (for station BULG; b, d), according to the SESAME criteria (*see Data and Resources*). The results are presented in terms of horizontal-to-vertical spectral ratio curves, HVSR, (a, b) and rotated HVSR (c, d).

Figure 6 - Topographic (a) and soil (b) classes (NTC, 2008; CEN, 2003), and their related geographic distributions (c, d, respectively). The statistics were performed for all the 213 seismic stations currently on ISMD.

Figure 7 - (a) Distributions of the assessed soil categories in the ISMD geological classes. (b) Distributions of the assessed topographic categories in the ISMD morphological classes. (c) Relationships between the assessed soil and topographic categories as now indicated in ISMD. The statistics were performed for all the 213 seismic stations currently available on ISMD.

Figure 8 - Distributions of the f_0 values in the adopted geological (a) and morphological (b) classifications. Here, the geological classes are grouped in *deposits* (i.e., *sedimentary*, *volcanic*, *morainic*, *debris-slope*) and *rock* (i.e., *sedimentary*, *metamorphic*, *igneous*), whereas the geomorphological classes in *flat* (i.e., *plain*, *plateau*, *valley*) and *slope* (i.e., *relief*, *ridge*, *gentle-slope*). For each subgroup, the assessed soil (a) and topographic (b) categories are also shown.

Table 1 - Strong-motion networks and relative number of stations now included in the ISMD web portal.

Net	Institute	Description	#
IV	INGV	Italian National Seismic Network (RSN)	172
XO	INGV temporary	Seismic Network for Site Effect Studies in Amatrice area	5
GU	University of Genova (DISTAV)	Regional Seismic Network of North Western Italy	7
TV	INGV temporary	INGV Experiment Network	3
MN	INGV in collaboration with other Institutions	Mediterranenan Very Broadband Seismographic Network - MEDNET	7
ST	Trento Province	Trentino Seismic Network	8
OX	OGS	North-East Italy Seismic Network	10
BA	University of Basilicata (UniBas)	Regional Seismic Network of Basilicata (Italy)	1

Table 2 - Soil categories, according to the current Italian seismic code for buildings (NTC, 2008). V_{S30}: average shear-wave velocity in the uppermost 30 m; $N_{SPT,30}$: standard penetration test blow-count; $c_{u,30}$: undrained shear strength of the soil.

Class	Description of stratigraphic profile	V_{S30} (m/s)	N_{SPT} (bl/30cm)	c_u (kPa)
A	Rock or other rock-like geological formation, including at most 3 m of weaker material at the surface	>800	-	-
B	Deposits of very dense sand, gravel, or very stiff clay, at least several tens of meters in thickness (> 30 m), characterised by a gradual increase of mechanical properties with depth	800-360	>50	>250
C	Deep deposits of dense or medium-dense sand, gravel or stiff clay with thickness from several tens to many hundreds of meters	360-180	50-15	250-70

D	Deposits of loose-to-medium cohesionless soil (with or without some soft cohesive layers), or of predominantly soft to-firm cohesive soil	<180	<15	<70
E	A soil profile consisting of a surface alluvium layer with Vs,30 values of class C or D and thickness varying between about 5 and 20 m, underlain by stiffer material with Vs,30 > 800m/s			
S1	Deposits consisting—or containing a layer at least 10 m thick of soft clays/silts with high plasticity index (PI > 40) and high water content	<100	-	10-20
S2	Deposits of liquefiable soils, of sensitive clays, or any other soil profile not included in classes A–E or S1			

662

663

664 **Table 3 -** Topographic categories, according to the current Italian seismic code for buildings (NTC,

665 2008).

Class	**Description**
T1	Flat surface, isolated slopes and cliffs with average slope angle $i < 15°$ or elevation difference H<30m
T2	Slopes with $i > 15°$ and elevation difference H>30m
T3	Relief with ridge top width much smaller than the base, and $15° < i < 30°$ and elevation difference H>30m
T4	Relief with ridge top width much smaller than the base, and $i > 30°$ and elevation difference H>30m

666

Figure1

Click here to download Figure Fig1.JPG

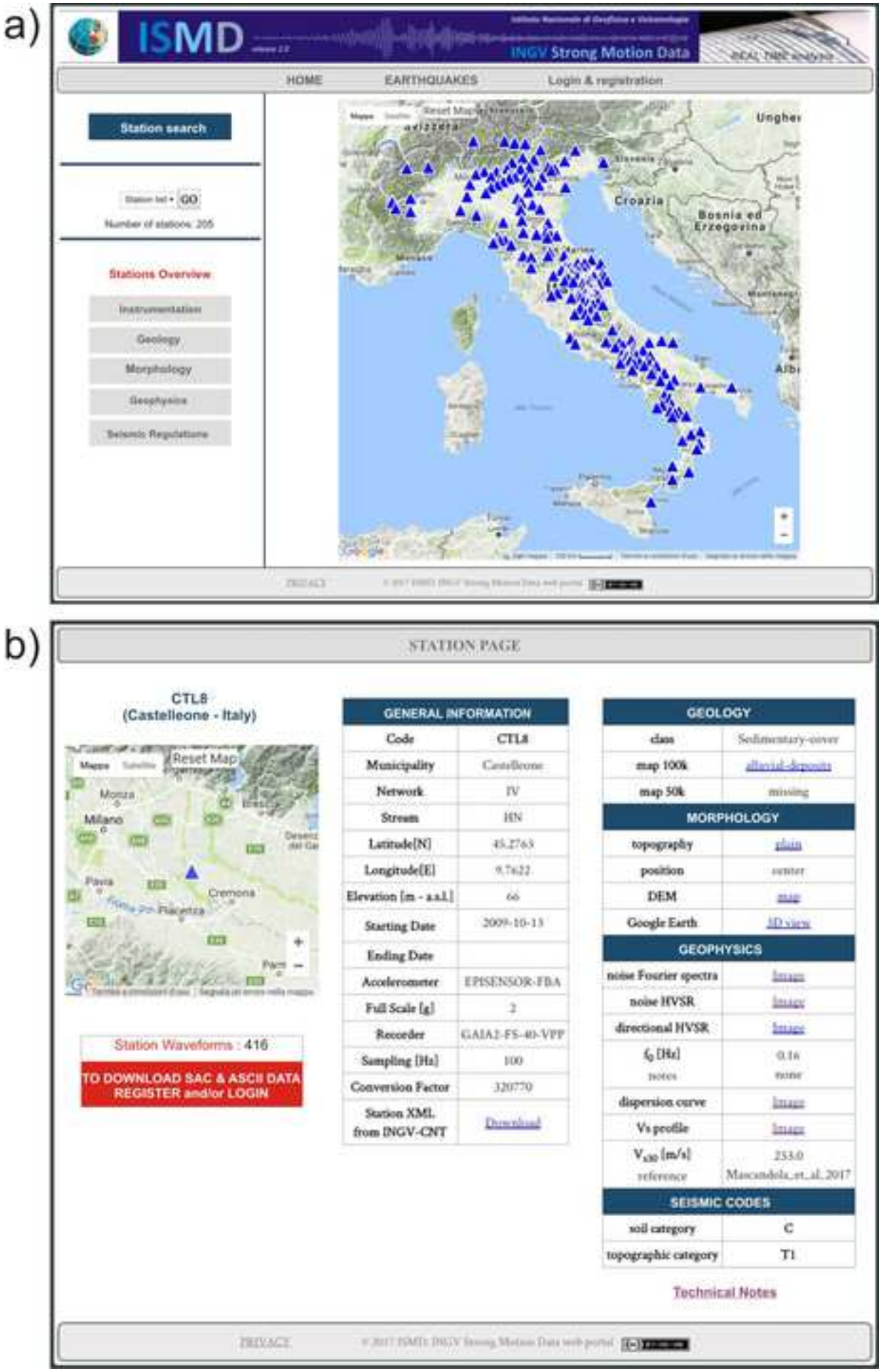

Figure2

Click here to download Figure Fig2.JPG

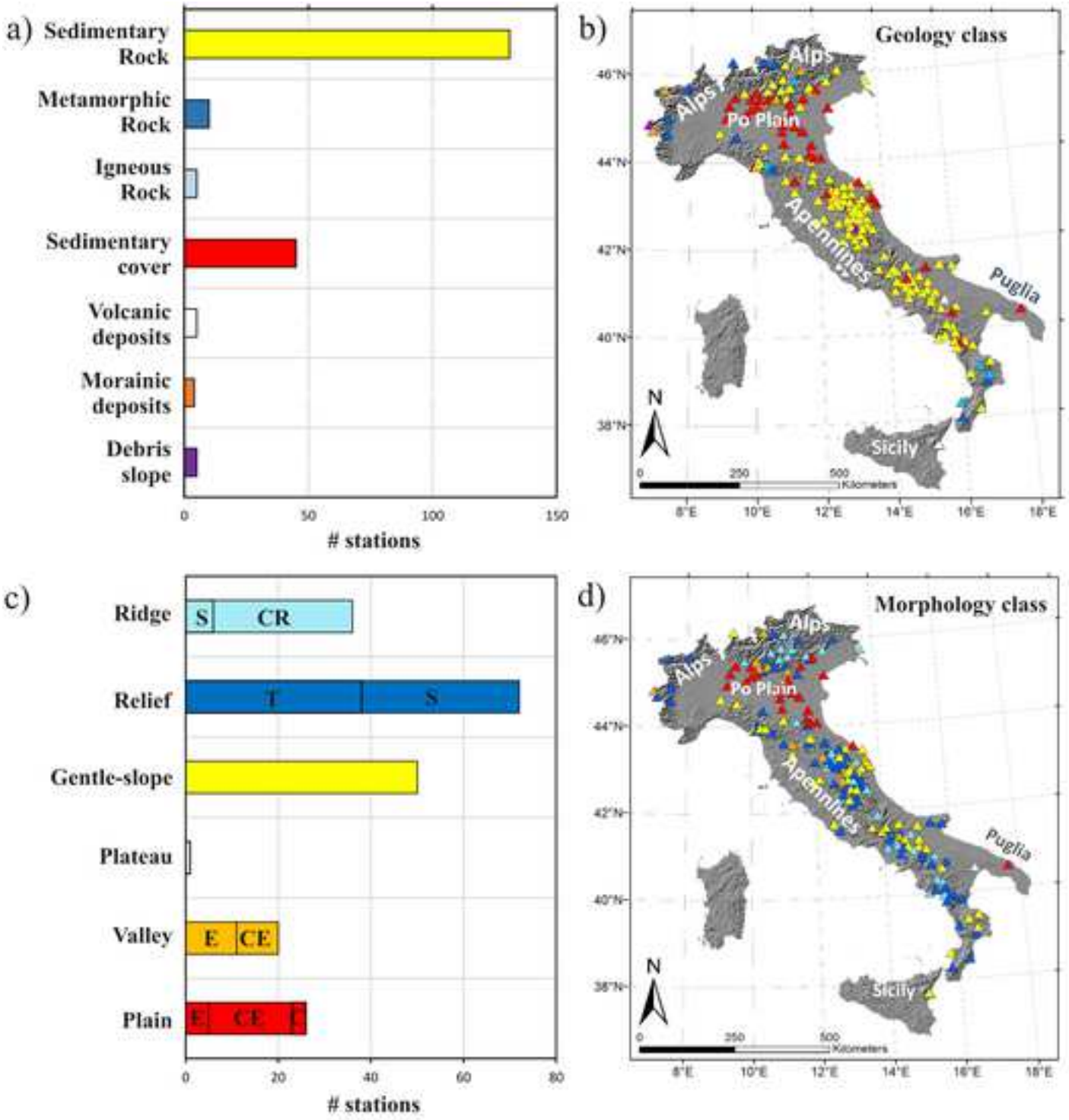

Figure3

Click here to download Figure Fig3.JPG

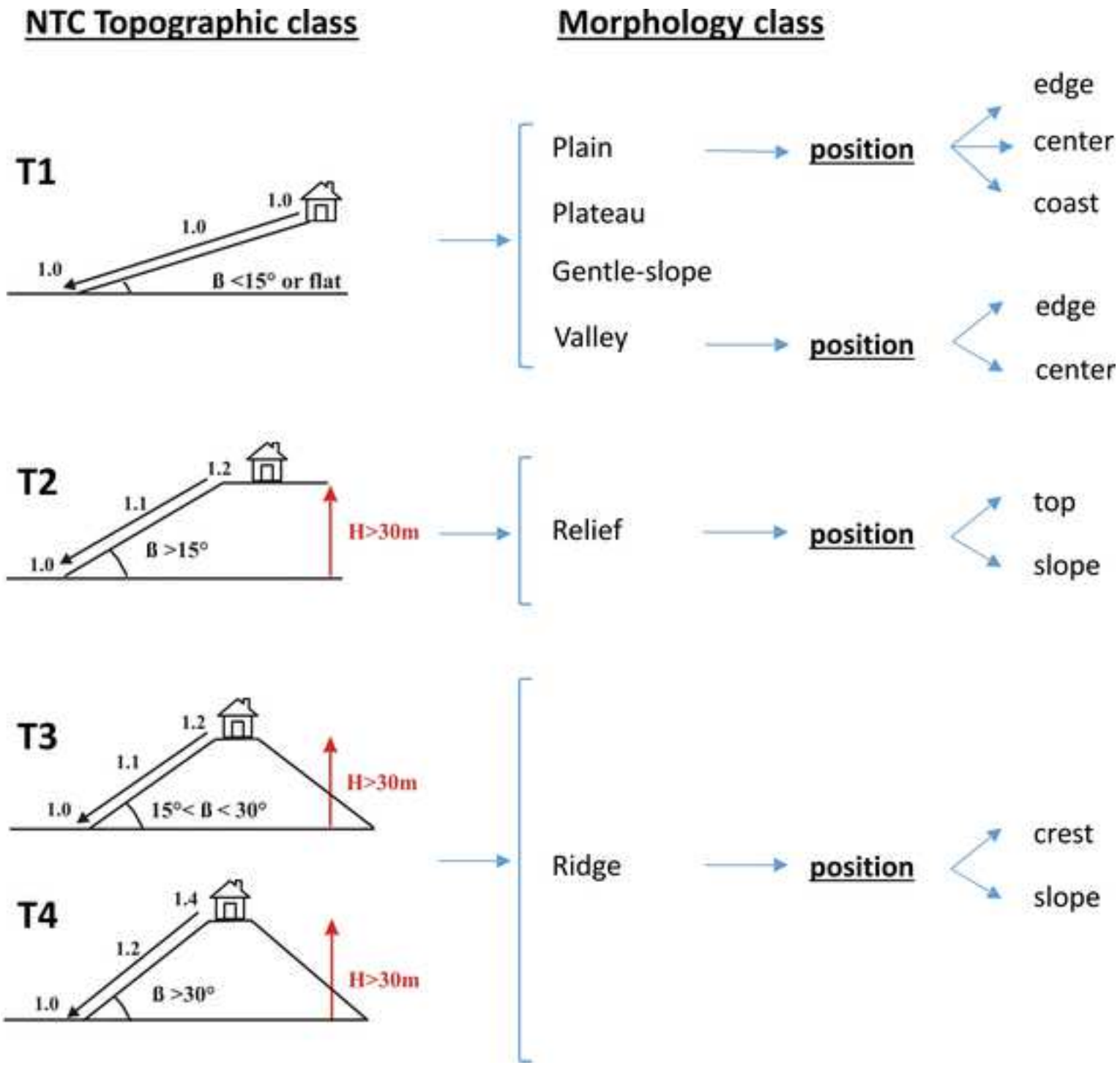

Figure4

Click here to download Figure Fig4.JPG

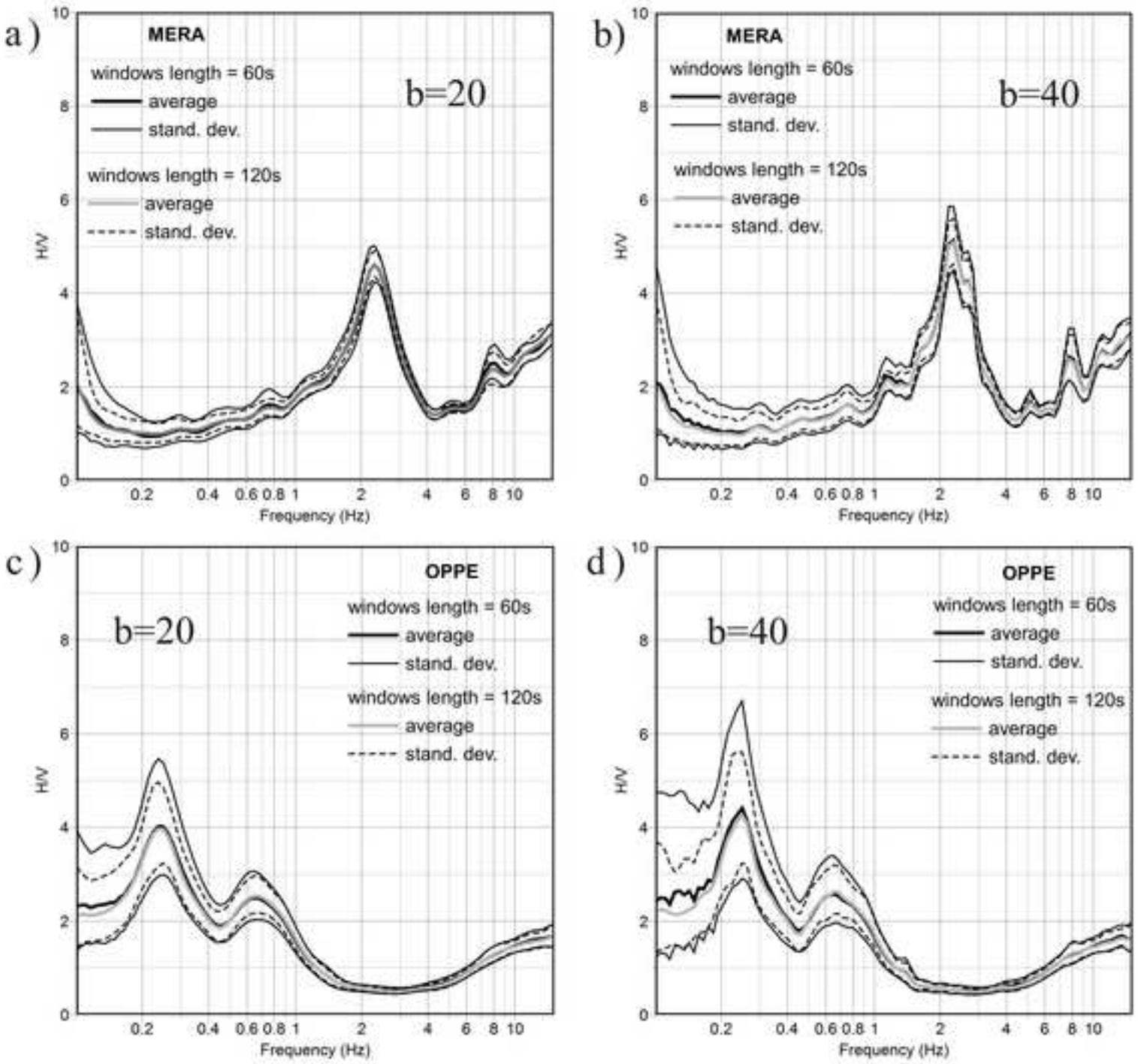

Figure5

Click here to download Figure fig5.JPG

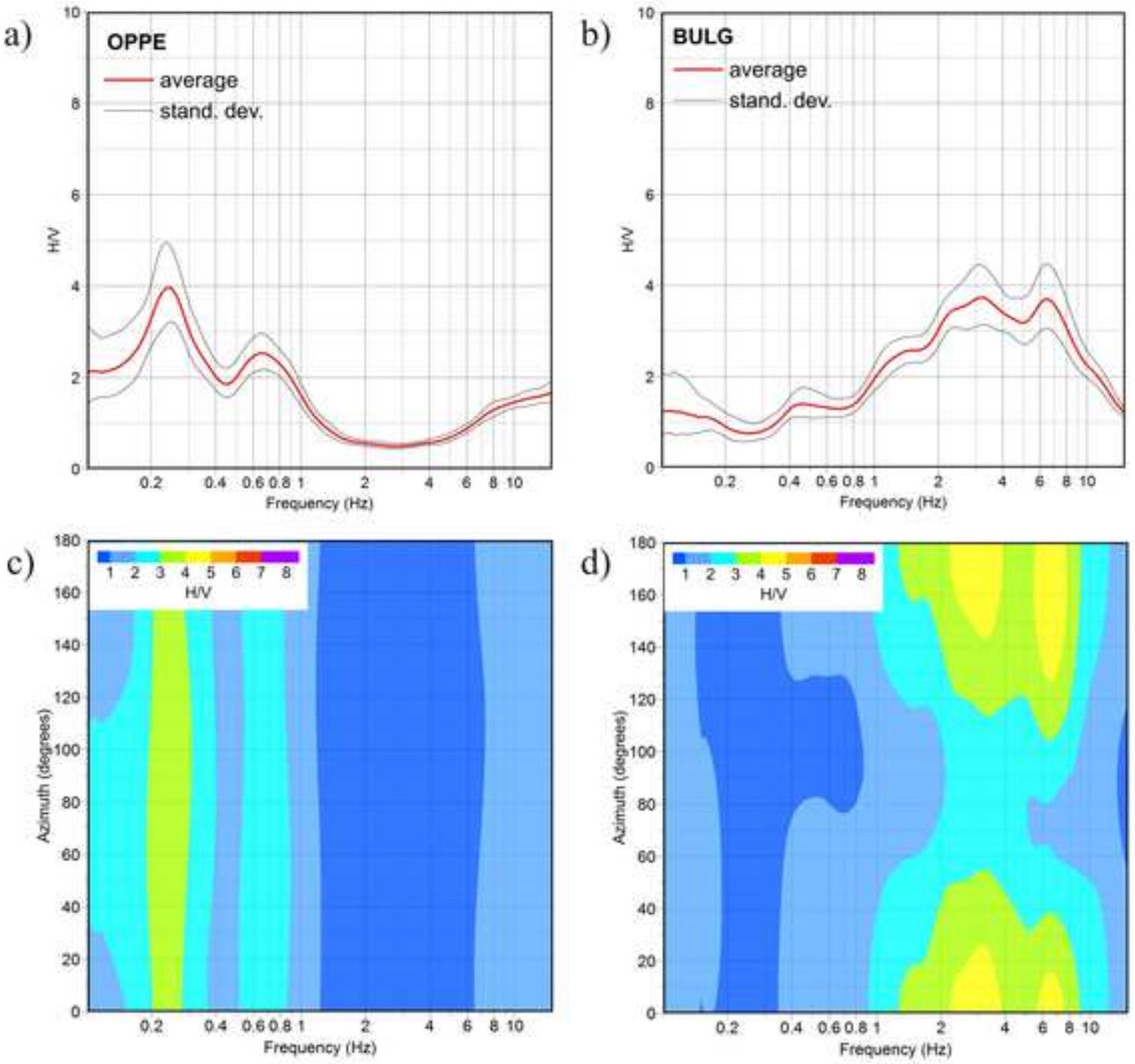

Figure6

Click here to download Figure Fig6.JPG

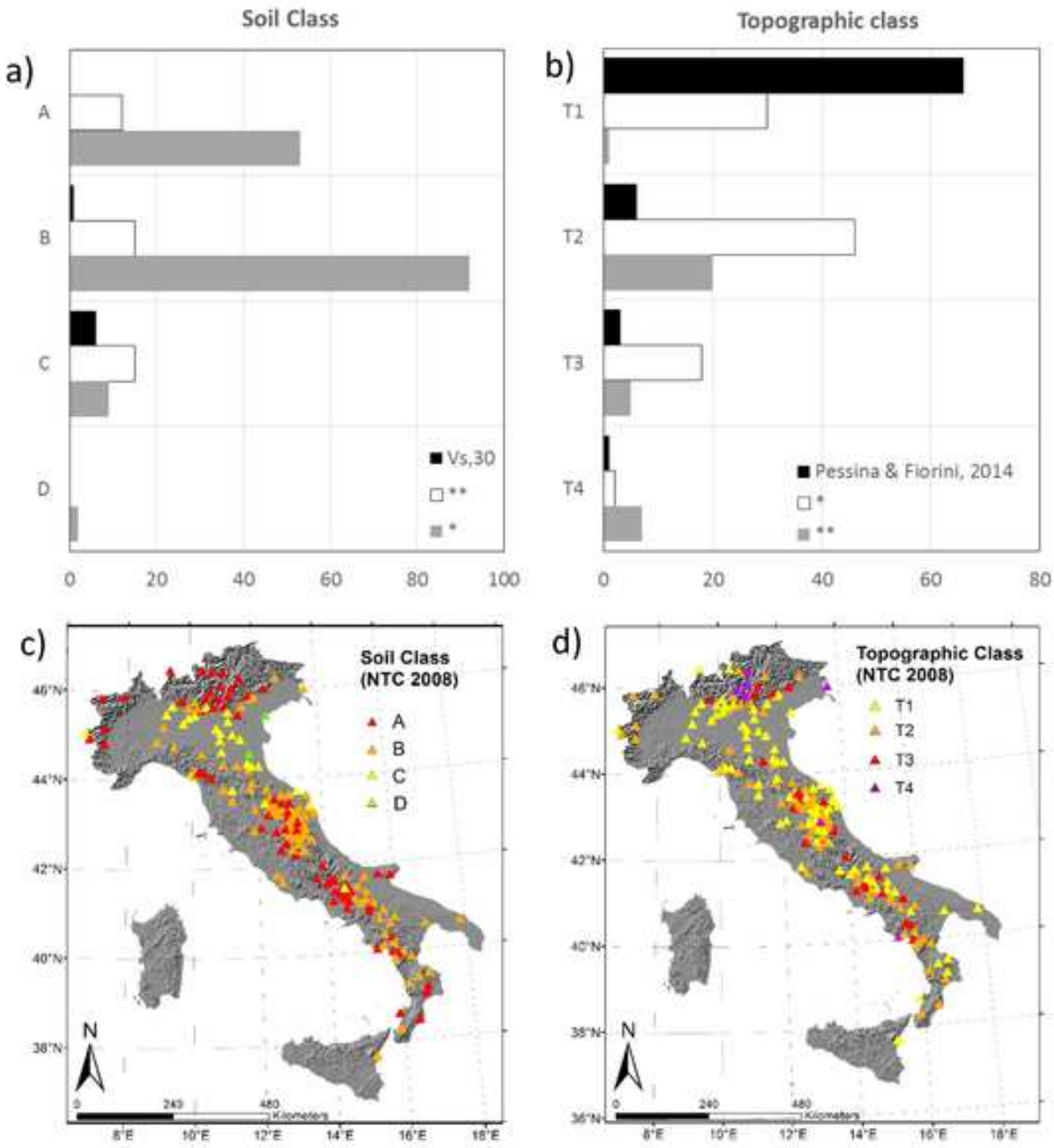

Figure7

Click here to download Figure Fig7.JPG

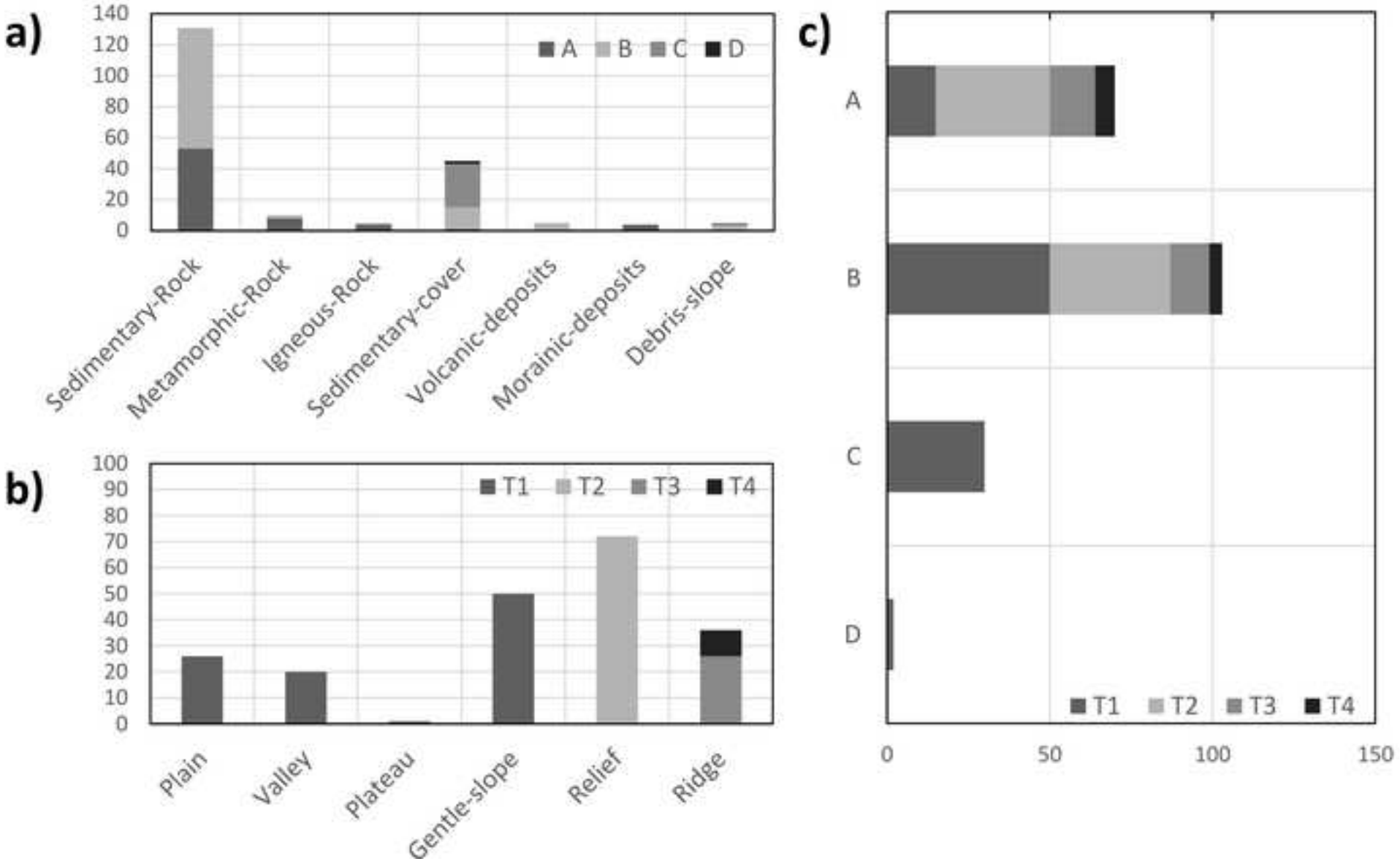

Figure8

Click here to download Figure Fig8.JPG

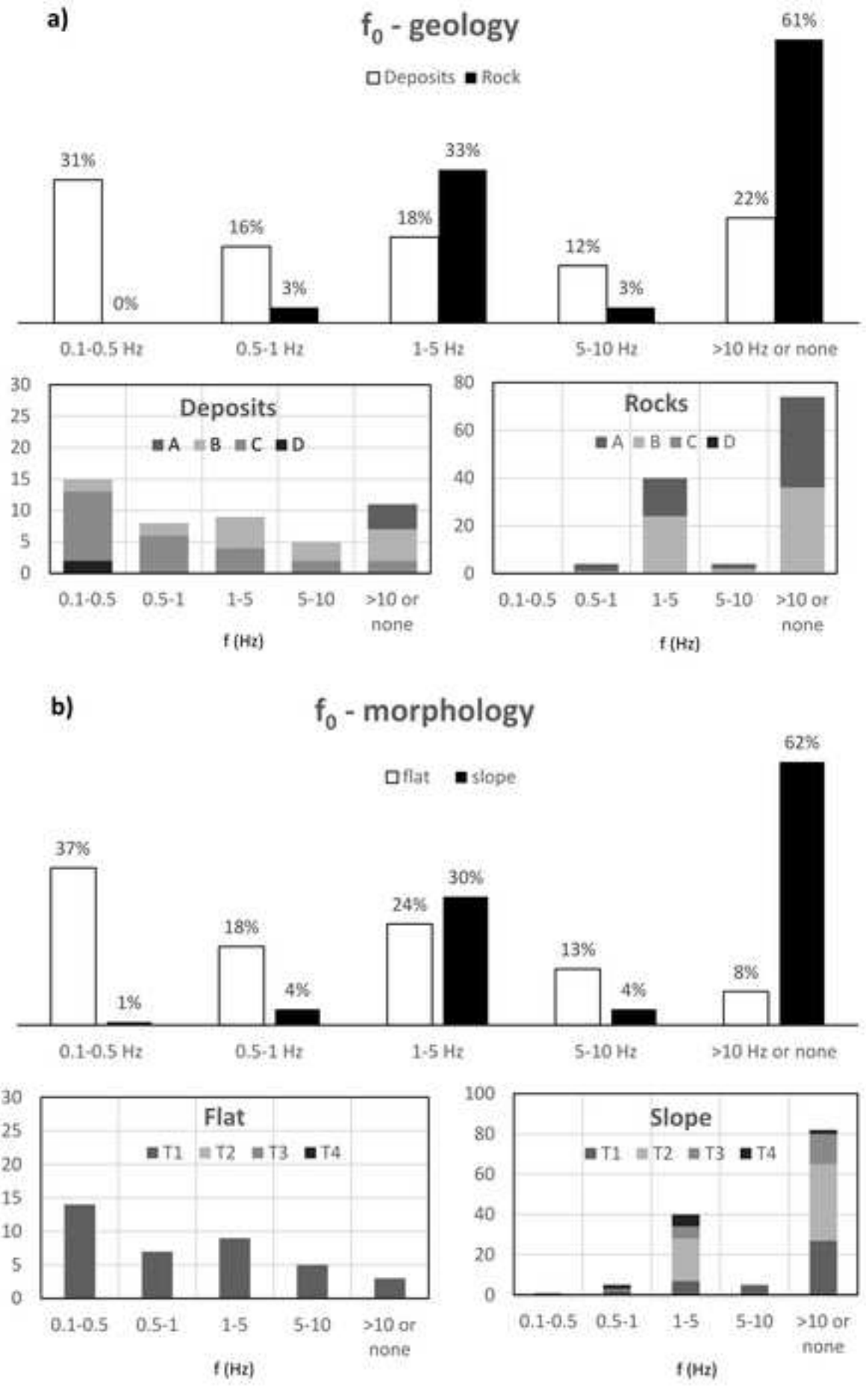

The site characterization scheme of the INGV Strong-Motion Database (ISMD): overview and site classification

Mascandola C.[(1)] *, Massa M.[(1)], Lovati S.[(1)], Augliera P.[(1)]

[(1)] Istituto Nazionale di Geofisica e Vulcanologia (INGV), Via Alfonso Corti 12, 20133, Milano, Italy

*** Corresponding author: claudia.mascandola@ingv.it**

Claudia Mascandola,

Istituto Nazionale di Geofisica e Vulcanologia

Via Alfonso Corti, 12

20133, Milano

Italy

Phone: +39 02 23699 653

Table S1- Soil and topographic categories assessed for the 213 strong-motion stations published on ISMD. The symbols * in column 7 (ISMD soil class) indicate the classes assigned on the basis of the available geological information (Di Capua et al., 2011). The symbol ** indicates the modifications with respect to Di Capua et al. (2011), made on the basis of an expert judgment (e.g. near measurements of V_S profiles or direct knowledge of the recording site). The topography classes in column 8 were assigned on the basis of the method proposed by Pessina and Fiorini (2014). The symbols * indicate the stations non-classified (i.e. *NC output*) by the considered method, while the symbols ** indicates further modifications performed after the visual inspection on Google Earth.

Table S1- Soil and topographic categories assessed for the 213 strong-motion stations published on ISMD. The symbols * in column 7 (ISMD soil class) indicate the classes assigned on the basis of the available geological information (Di Capua et al., 2011). The symbol ** indicates the modifications with respect to Di Capua et al. (2011), made on the basis of the expert judgment (e.g. near measurements of V_s profiles or direct knowledge of the recording site). The topography classes in column 8 were assigned on the basis of the method proposed by Pessina and Fiorini (2014). The symbols * indicate the stations non-classified (i.e. *NC output*) by the considered method, while the symbols ** indicates further modifications performed after the visual inspection on Google Earth.

Code	Net	Municipality	Lat. [°]	Lon. [°]	Elev. [m a.s.l.]	Soil class	Topo. class
ACER	IV	Acerenza	40.7867	15.9427	690	B*	T2*
ACOM	OX	Acomizza	46.5479	13.5149	1715	A*	T3*
AGOR	OX	Agordo	46.2829	12.0472	631	B**	T1*
AM01	X0	Amandola	42.9805	13.3587	549	B*	T4**
AM02	X0	Amandola	42.9795	13.3535	516	B*	T3*
AM03	X0	Amandola	42.9816	13.3627	511	B*	T4*
AM04	X0	Amandola	42.9833	13.365	455	B*	T3*
AM05	X0	Amandola	42.9774	13.3527	464	B**	T1*
APEC	IV	Apecchio	43.5584	12.4199	488	B**	T1
APRC	IV	Apricena	41.7573	15.543	672	A*	T2*
AQU	MN	LAquila	42.354	13.405	710	B**	T1
ASOL	IV	Asolo	45.8003	11.9023	181	B**	T2*
ASQU	IV	Asqua	43.7967	11.7893	860	B*	T2*
AT03	TV	Citta_di_Castello	43.5358	12.3859	789	B*	T2**
AT04	TV	Umbertide	43.2542	12.4504	595	B*	T2**
AT10	TV	Gubbio	43.3196	12.6942	571	B*	T1*
ATCC	IV	Casa_Castalda	43.1851	12.6399	557	B*	T2*
ATFO	IV	Monte_Foce_Gubbio	43.3666	12.5715	960	B*	T3
ATLO	IV	Monte_Lovesco	43.3151	12.4072	584	B*	T2**
ATPC	IV	Poggio_Castellaccio	43.4807	12.457	810	B*	T4**
ATTE	IV	Monte_Tezio	43.1979	12.3536	929	A*	T3*
ATVO	IV	Monte_Valentino	43.3821	12.4066	638	B*	T2*
BAG8	IV	Bagolino	45.8228	10.4664	807	A*	T2*
BDI	IV	Bagni_Lucca	44.0623	10.5969	830	A**	T2*
BHB	GU	Bricherasio	44.8352	7.2633	585	A*	T2*
BIOG	IV	Campo_Reale	41.1998	15.1326	623	B*	T1*
BNI	MN	Bardonecchia	45.052	6.678	1395	C**	T1
BOB	IV	Bobbio	44.7679	9.4478	910	B*	T1*

BORM	IV	Bormio	46.4694	10.3764	1235	A**	T1*
BOTM	IV	Botticino_Mattina	45.5416	10.3213	157	C**	T1
BOTT	IV	Botticino	45.5494	10.3095	200	A*	T2*
BRIS	IV	Brisighella	44.2245	11.7665	260	B*	T2*
BRSN	IV	Barisano	44.2841	12.0802	20	C**	T1
BSSO	IV	Busso	41.5461	14.5938	1010	A*	T2**
BULG	IV	Bulgheria_Camerota	40.0783	15.3776	815	A*	T4**
CADA	IV	Capodarco	43.1942	13.7614	148	B*	T1*
CAFE	IV	Carife	41.028	15.2366	1070	A*	T2**
CAFI	IV	Castiglion_Fiorentino	43.3292	11.9663	547	B*	T2*
CAPR	IV	Capriolo	45.6372	9.9345	215	B**	T1
CAR1	IV	Carolei	39.2534	16.2114	680	B*	T2*
CARE	ST	Lago_Careser	46.4252	10.6945	2605	A**	T2*
CDCA	IV	Citta_Castello	43.4584	12.2336	50	C**	T1
CEL	MN	Celeste	38.2603	15.8939	702	B*	T2*
CELI	IV	Lago_Cecita	39.4027	16.5088	1290	B*	T1*
CERA	IV	Filignano	41.5978	14.0183	800	A*	T1*
CGRP	OX	Cima_Grappa	45.8806	11.8047	1757	A*	T3**
CIMA	IV	Civitanova_Marche	43.3052	13.67	163	B*	T1*
CIMO	OX	Cimolais	46.3116	12.4448	710	B**	T1*
CLUD	OX	Cludinico	46.4569	12.8814	635	A*	T2*
CMPO	IV	Campotto_Po	44.5808	11.8056	2	D	T1
CNCS	IV	Concesio	45.606	10.217	126	B**	T1
COR1	IV	Corinaldo	43.6318	13.0003	237	B*	T1
CPGN	IV	Carpegna	43.8011	12.3205	1400	B*	T2**
CRM1	IV	Castel_Raimondo	43.21	13.058	302	C*	T1
CRMI	IV	Carmignano	43.7955	10.9795	490	B*	T2*
CRND	IV	Cornuda	45.8361	12.0131	159	B**	T1
CTL8	IV	Castelleone	45.2763	9.7622	66	C	T1
CUC	MN	Castrocucco	39.9938	15.8155	637	A*	T3
DOSS	ST	Dosso_Sommo	45.8808	11.1884	1660	A**	T3*
EPOZ	IV	Pozzillo	37.6719	15.1885	121	B**	T1
EUCT	IV	Pavia	45.2026	9.1349	82	B**	T1
EVRN	IV	Santa_Venerina	37.6892	15.1356	421	B**	T1
FAEN	IV	Faenza	44.2895	11.877	41	C*	T1
FEMA	IV	Monte_Fema	42.9621	13.0497	1370	B*	T2*
FERB	OX	Casaglia	44.9014	11.54	-135	C**	T1
FERS	IV	Casaglia	44.9035	11.5406	3	C	T1
FIAM	IV	Fiamignano	42.268	13.1171	1070	A*	T2*
FIR	IV	Firenze	43.7743	11.2551	40	C**	T1
FIU1	IV	Fiuminata	43.1885	12.9316	479	B**	T1*
FIVI	GU	Fivizzano	44.2393	10.1273	380	B	T2**
FOSD	GU	Fosdinovo	44.1076	9.9971	560	C*	T1
FOSV	IV	Fossato_di_Vico	43.2948	12.7611	559	B*	T2*
FRE8	IV	Fregona	46.0156	12.3551	545	A*	T3**
GAG1	IV	Gagliole	43.238	13.0674	484	B*	T3*

GAGG	ST	Gaggia	46.0835	10.9587	1617	A*	T4**
GATE	IV	Gambatesa	41.5131	14.9102	487	B*	T3*
GUMA	IV	Gualdo_Macerata	43.0627	13.3335	574	B*	T1*
IMOL	IV	Imola	44.3595	11.7424	27	C*	T1
INTR	IV	Introdacqua	42.0115	13.9046	924	A*	T3
JOPP	IV	Joppolo	38.6068	15.8856	500	A**	T1*
LAV9	IV	Lanuvio	41.6777	12.6988	300	B*	T2*
LEOD	IV	Capriano_Colle	45.4582	10.1234	93	C**	T1
LTRZ	IV	Laterza	40.6032	16.8191	381	B*	T1
MCEL	IV	Monticello	40.3249	15.8019	960	A*	T3*
MDAR	IV	Monte_Daria	43.1927	13.1427	940	B*	T3**
MDI	IV	Monte_di_Nese	45.7697	9.716	954	A*	T3*
MELA	IV	Melanico_S_Croce_Magliano	41.7059	15.127	115	B**	T1
MERA	IV	Merate	45.6725	9.4182	350	C**	T1
MESG	IV	Mesagne	40.5894	17.8504	78	B*	T1
MGAB	IV	Montegabbione	42.9126	12.1121	547	A*	T1*
MGR	IV	Morigerati	40.1376	15.5535	288	B*	T2*
MIDA	IV	Miranda	41.6418	14.254	950	A*	T2*
MILN	IV	Milano	45.4803	9.2321	125	C	T1
MMO1	IV	Montemonaco	42.8993	13.3268	982	B*	T2*
MMUR	IV	Monte_Murano	43.4418	12.9973	800	A*	T2**
MNS	IV	Montasola	42.3854	12.681	706	A*	T3*
MNTP	IV	Montappone	43.1373	13.4692	325	B*	T1
MNTV	IV	Mantova	45.1495	10.7897	38	C**	T1
MOCO	IV	Biccari_Monte_Cornacchia	41.37	15.158	1049	B*	T1*
MODE	IV	Modena	44.6297	10.9491	41	C**	T1
MOMA	IV	Monte_Martano	42.801	12.5681	1040	A*	T2*
MPAG	IV	Monte_Paganuccio	43.6292	12.7595	930	B*	T2**
MPRI	OX	Monte_Prat	46.2408	12.9877	762	B*	T2**
MRB1	IV	Monte_Rocchetta	41.1227	14.9681	688	B*	T3*
MRLC	IV	Muro_Lucano	40.7564	15.4889	605	B*	T2*
MSAG	IV	Monte_S_Angelo	41.712	15.9096	890	A*	T2**
MTL1	IV	Matelica	43.2567	13.0096	353	C*	T1
MTMR	IV	Montemarano	40.9184	15.0025	850	B**	T1*
MTRZ	IV	Monterenzio	44.3128	11.4248	570	B*	T3*
MURB	IV	Monte_Urbino	43.263	12.5246	845	B*	T2**
NDIM	IV	Novi_Mo	44.8873	10.8987	19	C	T1
NEV1	IV	Neviano_Arduini	44.5834	10.3163	480	B*	T1**
NEVI	IV	Neviano_Arduini	44.5834	10.3163	480	B*	T2
NRCA	IV	Norcia	42.8335	13.1142	927	B**	T1*
OPPE	IV	Oppenano	45.3082	11.1723	20	C*	T1
ORZI	IV	Orzinuovi	45.4056	9.9307	83	C*	T1
OSSC	IV	Zona_Poggibonsi	43.5235	11.2457	452	B*	T1
OZOL	ST	Ozolo	46.404	11.0518	1219	A*	T4**
PANI	ST	Panarotta	46.0501	11.3341	1983	A**	T3*
PAOL	IV	Paolisi	41.0312	14.5674	715	A*	T2*

PCRO	IV	Pietra_Croce	43.6076	13.5323	165	B*	T1
PIEI	IV	Pieia	43.5356	12.535	665	A*	T3*
PIGN	IV	Pignataro_Maggiore	41.2	14.1798	398	A*	T3*
PIO1	IV	Pioraco	43.1781	12.9837	460	B*	T1*
PIPA	IV	Pietra_Paola	39.4851	16.8158	479	B*	T1*
PLAC	IV	Placanica	38.4494	16.4383	602	A*	T2*
POFI	IV	Posta_Fibreno	41.7174	13.712	878	A*	T1
PP3	IV	Macerata	43.3778	13.6095	21	C**	T1
PSB1	IV	Pesco_Sannita	41.2234	14.8107	551	B*	T1
PTRJ	IV	Pietraroja	41.3641	14.529	1027	A*	T2*
PZUN	BA	Potenza	40.6458	15.807	820	B*	T1
REMY	GU	Saint_Rhemy_en_Bosses	45.8378	7.1565	2448	A**	T2*
RM33	IV	zona_Paganica	42.5089	13.2145	1097	B*	T2*
RNI2	IV	Rionere_Sannitico	41.7032	14.1524	950	A*	T1*
ROM9	IV	Roma_sede	41.8284	12.5155	110	B*	T1
RONC	ST	Roncone	45.9802	10.6228	1913	A**	T4**
ROVR	IV	Rovere_Veronese	45.6468	11.0721	1316	A*	T2**
RRL	GU	Rocca_Remolon	44.921	6.79	2175	A**	T2*
RSP	GU	Reno_Superiore	45.1481	7.2653	1285	A**	T2
SABO	OX	M_Sabotino	45.9875	13.6336	621	B*	T4*
SACR	IV	S_Croce_Sannio	41.3974	14.7057	859	A*	T1
SACS	IV	San_Casciano_Bagni	42.849	11.9096	845	B*	T1
SALB	IV	San_Lorenzo_Bellizzi	39.8772	16.3459	1200	B*	T2**
SALO	IV	Salo	45.6183	10.5243	600	A*	T2*
SANR	IV	Sandrigo	45.64	11.6099	51	C	T1
SARZ	IV	Sarezzano	44.8673	8.9136	266	B*	T1
SATI	GU	Passo_Salati	45.8753	7.8685	3005	A*	T2*
SBPO	IV	San_Benedetto_Po	45.051	10.9198	10	C**	T1*
SEF1	IV	Sefro	43.1468	12.9476	518	A*	T1*
SENI	IV	Senigallia	43.7052	13.2331	10	C*	T1
SERM	IV	Semide	45.0099	11.2958	7	C**	T1
SERS	IV	Sersale	39.0359	16.6886	1221	A**	T2*
SFI	IV	S_Sofia	43.9047	11.8469	548	B*	T1*
SGG	IV	San_Gregorio_Matese	41.3867	14.3791	880	A*	T2*
SGTA	IV	Sant_Agata_Puglia	41.135	15.365	890	B*	T1
SIRI	IV	Monte_Sirino_Moliterno	40.1821	15.8675	1063	B*	T2*
SLCN	IV	Sala_Consilina	40.39	15.6327	986	B*	T3**
SNAL	IV	San_Angelo_Lombardi	40.9254	15.209	874	A*	T2*
SNTG	IV	Esanatoglia	43.255	12.9405	650	A*	T2
SSFR	IV	Montelago_Sassoferrato	43.4362	12.7822	750	A*	T1
SSM1	IV	San_Severino_Marche	43.2287	13.1769	240	B*	T1
STAL	IV	Staligial	46.2601	12.7104	625	B*	T2
T0104	IV	Coppito	42.3599	13.3382	754	B*	T2**
T0701	IV	Pollino	39.9861	16.1161	882	B*	T2*
T0721	IV	Laino_Castello	39.9369	15.9769	535	A*	T2**
T0724	IV	Tremoli	39.8487	15.8764	357	B*	T2*

T0819	IV	Novi_Mo	44.8873	10.8987	19	C	T1
T0821	IV	Casaglia	44.9035	11.5406	3	C	T1
T0911	IV	Castelpoggio	44.1117	10.0737	520	B*	T2*
T0912	IV	Milucciano	44.1685	10.2095	687	A*	T1*
T1011	IV	San_Potito_Sannitico	41.3596	14.4174	1152	A*	T3*
T1012	IV	Faicchio	41.2623	14.4965	599	A*	T3*
T1101	IV	Campobasso	41.4746	14.536	510	C**	T1
T1201	IV	Domo	42.6573	13.2508	934	B*	T2**
T1211	IV	Morro_Reatino	42.5328	12.8551	979	A**	T2
T1212	IV	Cascia_Avendita	42.7515	13.0446	869	B*	T1
T1213	IV	Norcia_Savelli	42.7249	13.1257	860	B*	T1
T1214	IV	Arquata_del_Tronto	42.7595	13.2086	1490	A*	T1
T1215	IV	Reggiano	42.8018	12.8685	695	B*	T1*
T1216	IV	Castelvecchio	42.8906	13.019	620	B*	T1*
T1217	IV	Poggiodomo	42.7119	12.9313	1004	B*	T2*
T1218	IV	Civita	42.6699	13.1152	1184	B**	T1
T1219	IV	Massaprofoglio	43.0558	13.0047	717	B*	T1
T1220	IV	Baregnano	43.1101	13.0889	474	B*	T1
T1221	IV	Spina_Nuova	42.8561	12.8414	951	A*	T1
T1222	IV	Castel_S_Angelo_sul_Nera	42.4013	13.0367	556	B*	T1*
T1241	IV	Osoli	42.8563	13.4311	664	B*	T2**
T1242	IV	Castelluccio_Norcia	42.8292	13.2043	1451	A*	T2**
T1243	IV	Ceppo_Pietralta	42.6965	13.4483	1120	B*	T2*
T1244	IV	Spelonga	42.7569	13.2977	950	B*	T2*
T1245	IV	Castel_S_Angelo_sul_Nera	42.8565	13.1879	1541	A**	T4
T1256	IV	Sassotetto	43.0063	13.226	1536	A*	T2
T1299	IV	Amatrice	42.6342	13.2822	940	B*	T1*
TERO	IV	Teramo	42.6227	13.6039	673	B*	T3*
TIP	MN	Timpagrande	39.1794	16.7583	789	A**	T1*
TRE1	IV	Treia	43.3111	13.3128	330	B*	T3**
TREG	IV	Tregnago	45.5229	11.1606	342	C**	T1
TRIV	IV	Trivento	41.7666	14.5502	598	B*	T1
TUE	MN	Stuetta	46.4722	9.3473	1924	A*	T1*
VAGA	IV	Valle_Agricola	41.4154	14.2342	795	A*	T2*
VARA	ST	Varagna	45.826	10.8965	1735	A*	T4**
VARN	OX	Varnada	45.9933	12.1048	1265	A*	T3*
VENL	IV	Venezia_Lido	45.4167	12.3765	4	D*	T1
VITU	IV	Vitulano	41.1832	14.6301	848	A*	T2*
VLC	MN	Villacollemandina	44.1594	10.3864	555	A*	T1
VOBA	IV	Vobarno	45.6429	10.504	292	C*	T1*
VULT	IV	Monte_Vulture	40.9549	15.6163	1101	B*	T3*
ZCCA	IV	Zocca	44.3508	10.9765	700	B*	T1*
ZEN8	IV	San_Zeno_Montagna	45.6378	10.7319	596	A**	T2**
ZIAN	ST	Ziano	46.2764	11.5632	1154	A**	T2*
ZONE	IV	Zone	45.7636	10.1171	691	B*	T1
ZOU2	OX	Zouf_Plan	46.5584	12.9729	1911	B*	T4*

ZOVE	IV	Zovencedo	45.4536	11.4876	376	A**	T2**